# Variations in the Structure of the Equatorial Anomaly during the Summer Solstice according to the Interkosmos-19 Satellite

**A. T. Karpachev***

*Institute of Terrestrial Magnetism, Ionosphere and Radio Wave Propagation, Moscow, Russia*
**e-mail: karp@izmiran.ru*

**Abstract**—Changes in the structure of the summer equatorial anomaly of electron density with local time and longitude at high solar activity are considered in detail according to topside sounding data from the Interkosmos-19 satellite. It is shown that the equatorial anomaly starts to develop from ~0800 LT, when the winter (southern) crest is formed. The summer (northern) crest is ~2 h behind in development. It is formed at the background of a low latitudinal $foF2$ maximum. In the daytime, the northern crest is ~3° farther from the geomagnetic equator than the southern one. The crest position changes greatly with longitude. A local maximum is observed in the development of the equatorial anomaly at 1400 LT. It is particularly pronounced in the Eastern Hemisphere. The $foF2$ value above the geomagnetic equator and anomaly intensity change with longitude at 1200−1400 LT according to the changes in the vertical plasma drift $W$. A local minimum is observed in the development of the equatorial anomaly at 1800 LT. The anomaly intensity then increases to a maximum 1.5−2.0 h after the evening peak in $W$. Longitudinal $foF2$ variations and the anomaly intensity in the interval 2000−2200 LT are also associated with $W$ variations. The anomaly intensity decreases after the maximum, and the crests decrease in magnitude and move toward the equator. The $foF2$ maxima in the crest region of the anomaly after midnight, conversely, are farther away from the geomagnetic equator, which seems to be due to the action of the neutral wind. The equatorial anomaly has almost decayed by 0400 LT and does not manifest itself as a structure from 0500 to 0700 LT. Therefore, the well-expressed equatorial anomaly is observed from 1200 to 2400 LT at high solar activity.

## 1. INTRODUCTION

An equatorial anomaly (EA) in electron density was detected long ago (Appleton, 1946) and has been studied with the use of both ground-based and satellite data. The ground-based data are limited in both latitude and, especially, longitude, because they are typically obtained in three longitudinal sectors: Asian, American, and sometimes African (e.g., Thomas, 1968; Rajaram, 1977; Walker, 1981; Eccles and King, 1969; Rao and Malthotra, 1964; Lyon and Thomas, 1963; Rush et al., 1969). The satellite data are obtained either at a fixed height above the maximum of the $F2$ layer with a Langmuir probe or over the entire thickness of the topside ionosphere with sounding from above. In situ measurements primarily include data from the CHAMP satellite, the orbit of which, while gradually lowering, was close to the maximum of the $F2$ layer at heights of 465−300 km (Liu et al., 2007; Lei et al., 2010), as well as data obtained from the Ariel (Hopkins, 1972) and ROCSAT (Chen et al., 2016) satellites at heights of 500−600 km and 600 km, respectively. Several studies were carried out with the use of topside sounding data from the Alouette and ISIS satellites, which were also associated with telemetry sta-

tions only in the Asian and American longitudinal sectors (Sharma and Hewens, 1976; Eccles and King, 1969; Lockwood and Nelms, 1964; King et al., 1967; Rush et al., 1969). Despite the limitations, all of these observations made it possible to find the main features of the EA described in the reviews (Rajaram, 1977; Moffett, 1979; Walker, 1981; Sastri, 1990; Rishbeth, 2000; Walker et al., 1994). It was shown that the EA characteristics vary greatly with height, longitude, local time, season, and solar activity. Diurnal and seasonal variations, as well as their dependence on solar activity, can be studied by any method. The dependence on height was studied mainly based on topside sounding data. Finally, the dependence on longitude can be fully identified only with satellite data.

This article studies the EA structure in $foF2$ based on topside sounding data from Interkosmos-19 (IK-19) averaged for the northern summer, i.e., May−August. So far, IK-19 has been the only satellite to record the global (at all longitudes) distribution of electron density, including $foF2$ and $hmF2$ variations, at high solar activity. IK-19 operated in 1979−1982, but the laborious primary processing of topside sounding data has been conducted methodically, i.e., in full, only in
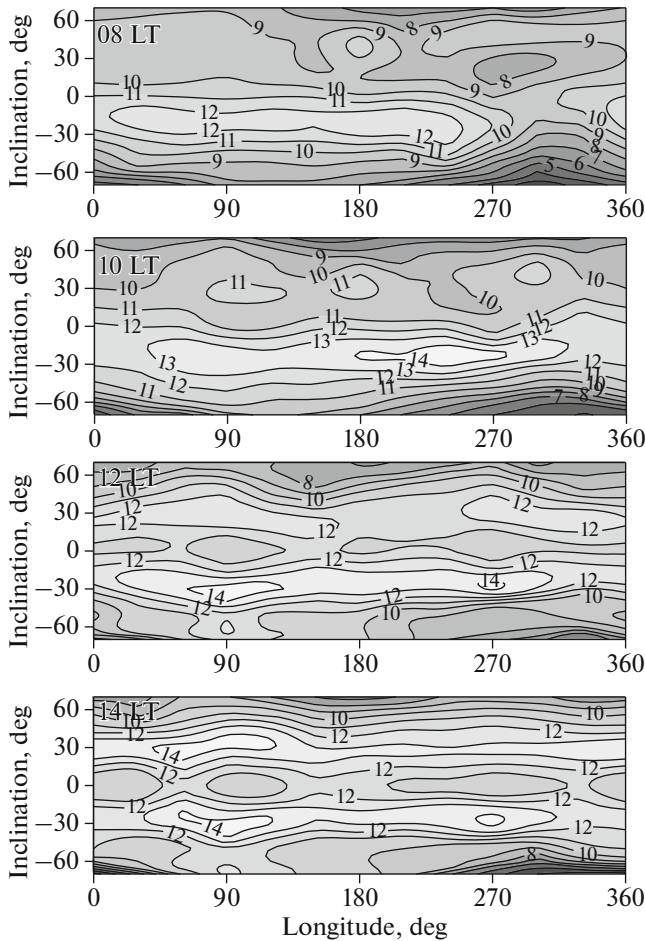
**Fig. 1.** Distribution of *foF*2 (LT-maps) during the period of EA development at 0800, 1000, 1200, and 1400 LT.

recent years. This made it possible to obtain a complete pattern of EA structure variations in quiet geomagnetic conditions for all local hours and all seasons. A detailed study of EA characteristics for equinoctial conditions was presented in our previous article (Karpachev, 2018). Below is a similar study for summer solstice conditions.

The main purpose of this article is to create a comprehensive pattern of the EA structure variations. Therefore, as not to overload the article, only the results that are directly related to the subject matter of analysis will be referred to throughout the text. This primarily applies to ground-based data. A lot of data on total electron content (TEC) have been recently obtained from GPS receivers. They are also ground-based and are not directly related to *foF*2 variations. Nevertheless, several important results will be used in the comparison with IK-19 data (Huang and Cheng, 1996; Yizengaw et al., 2009; Zhao et al., 2009). Finally, a huge amount of radio occultation data has been obtained, especially in the FORMOSAT-3/COSMIC experiment. These data are global, but they cover a

period of mainly low solar activity. However, they are also of interest, because they reveal the general EA structure for different solar activity conditions (Ram et al., 2009; Luan et al., 2015; Yue et al., 2015).

## 2. OBSERVATIONAL DATA

The IK-19 satellite was active from March 1979 to February 1981. This period was characterized by high solar activity with an average of $F_{10.7} \sim 200$. The satellite was in elliptical orbit with altitudes of 500−1000 km and an inclination of 74°. The satellite had a recording device on board for the digital recording of ionograms at any longitude within the orbital inclination. The ionograms were used to calculate the $N(h)$ profiles of the topside ionosphere, which provided the *foF*2 and *hmF*2 values. These values were used to plot the distribution of the maximum parameters of the $F2$ layer in the EA region within the limits of ±70° geomagnetic inclination. The summer conditions include May–August 1979 and 1980, i.e., 8 months for 2 years of satellite operation. A total of 87000 pairs of *foF*2 and *hmF*2 values for quiet conditions $Kp \leq 3$ were obtained during this period. This was sufficient to construct 12 so-called LT maps for every 2 h of local time. Every map has from 3000 to 4000 *foF*2 or *hmF*2 values. The maps were constructed with the Surfer software by the inverse distance method. The data for each map evenly covered all longitudes. As a result, a fairly smooth *foF*2 and *hmF*2 distribution was obtained, and it indirectly confirms the adequacy of the obtained data. This article considers only *foF*2 variations.

## 3. EA DEVELOPMENT

Figure 1 shows the *foF*2 distribution during EA development, i.e., for 0800, 1000, 1200, and 1400 LT, and Fig. 2 shows the latitudinal *foF*2 profiles in the most typical longitudinal sectors of 90° and 300°. The geomagnetic equator is located as far north as possible in the former sector and, conversely, to the south in the latter. From both figures it can be seen that the winter, i.e., southern, crest appears first, at 0800 LT. It emerges at a latitude of ~10° in the American longitudinal sector and at ~20° at other longitudes. In the Northern Hemisphere, there is a small *foF*2 maximum at all longitudes at this time, but it is too far away for a normal EA crest formed by a fountain effect. As a result, the *foF*2 minimum is shifted to the summer hemisphere, and this is not an equatorial density trough associated with the EA.

The northern (summer) crest starts to form only at 1000 LT and only at longitudes of 90°−210°. There is no summer crest at other longitudes, which is especially true for American longitudes, as shown by the latitudinal *foF*2 section in Fig. 2 for 1000 LT in the longitudinal sector of 300°. The *foF*2 peak at longitude 300° is still a low-latitude or even midlatitude maximum that is most likely caused by the action of the
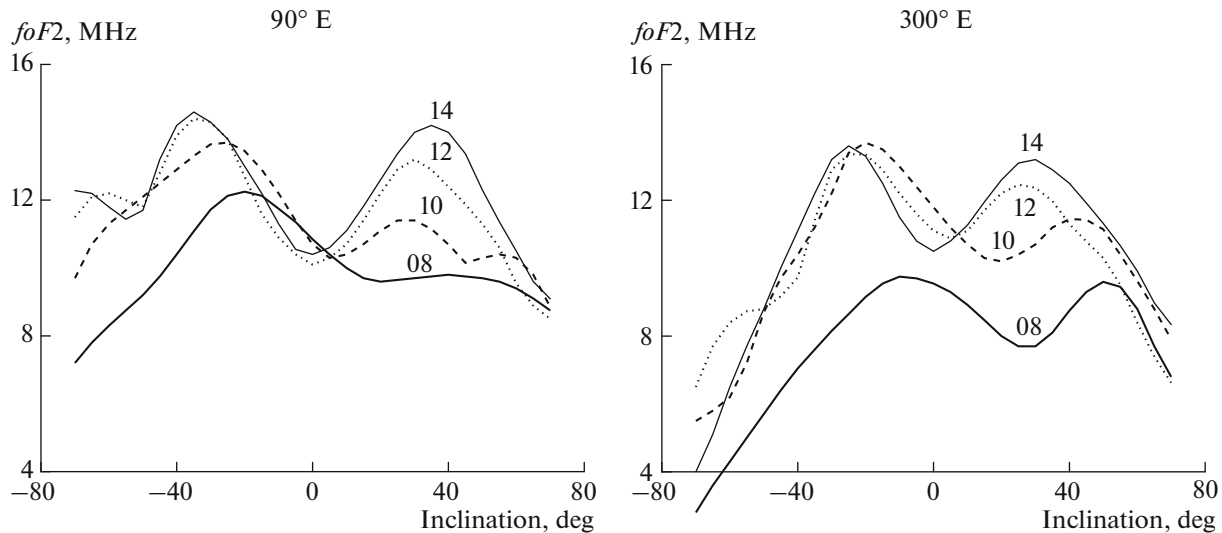
**Fig. 2.** Latitudinal *foF*2 variations at 0800, 1000, 1200, and 1400 LT in the most characteristic longitudinal sectors of 90° and 300°.

neutral wind. The latitudinal *foF*2 profile at a longitude of 90° shows the complex dynamics of the northern crest. It can be seen that it forms at the background of mid-latitude *foF*2 maximum. The northern crest at all longitudes forms only by 1100 LT. It reaches that of the winter crest closer to noon, and it is slightly smaller than the southern, winter crest even at 1400 LT. Therefore, the EA in its usual form, with two well-developed crests, forms only by noon in summer, at high solar activity. By this time, the EA is best developed at longitudes of 90°–120° as compared to other longitudes. In the American longitudinal sector, the EA is not only weaker, but it also forms later (Fig. 2).

Carry out a comparison with other data. Based on ground-based data, Walker (1981) argued that the winter crest develops earlier and is larger at any solstice and in any longitudinal sector. However, Walker and Chan (1976) previously analyzed the topside sounding data from Alouette-2 and ISIS-1 for November 1969–January 1970, i.e., at high solar activity, in the 105° sector, and found inverse asymmetry: during the daytime, the summer (southern) crest was 8% larger and 8° DIP farther away from the equator. Similarly, the summer crest prevailed according to Alouette-1 data obtained for low solar activity in November 1962 and June 1963 at the meridian of 75° W (Rush et al., 1969). As for the delay in EA development at American longitudes, it was noted in many early studies. However, analysis shows that these are mainly related to low solar activity and/or the equinox (e.g., Sharma and Hewens, 1976; Lyon and Thomas, 1963). For summer conditions of high activity, this was only noted in studies based on ground-based (Rajaram, 1977) and satellite (Hopkins, 1972) data, although the latter article also considered mixed conditions (July 7–October 18). Moreover, Thomas (1968) affirmed from ground-based data for the summer of 1958 that the EA was observed

in the American sector already at 0800 LT and appeared in the African sector only by 1200 LT. At the same time, the northern crest was larger during the daytime (1400 LT) in the African sector. Therefore, a rather controversial picture emerges from the early results. There are no later EA studies in terms of *foF*2 for summer conditions of high activity. We can only note the analysis of the TEC in the Asian–Australian region (Zhao et al., 2009). TEC variations show quite clearly that the winter crest appears and decays earlier at high activity ($F_{10.7} > 150$) than the summer crest in both summer and winter solstices. Apparently, this conclusion should be considered definitive.

Both crests gradually move away from the equator as the EA develops. The maximum latitude at 1400 LT depends on longitude and is in the range 23°–33° *I* in the Northern Hemisphere and 1°–2° lower in the Southern Hemisphere. The dependence of the magnitude and crest positions on longitude was also discussed in detail in many studies (e.g., Walker, 1981). It is determined mainly by the action of both neutral wind components. The meridional wind is directed to the pole from the subsolar point. Therefore, it will act differently on the EA crests depending on the season and the displacement between geographical and geomagnetic equators. It reduces them in one case and increases in the other. The action of the zonal wind depends on the inclination of the geomagnetic field. The inclination sign changes its effect (at fixed local time) to its opposite. Lastly, the location of the subsolar point is also important, i.e., where ionization by solar radiation is stronger during the daytime. However, although the difference in longitude in the crest position reaches 10°, there is no strong asymmetry on average either in magnitude or in the crest position. This conclusion is quite unexpected, because many studies emphasize strong EA asymmetry during the
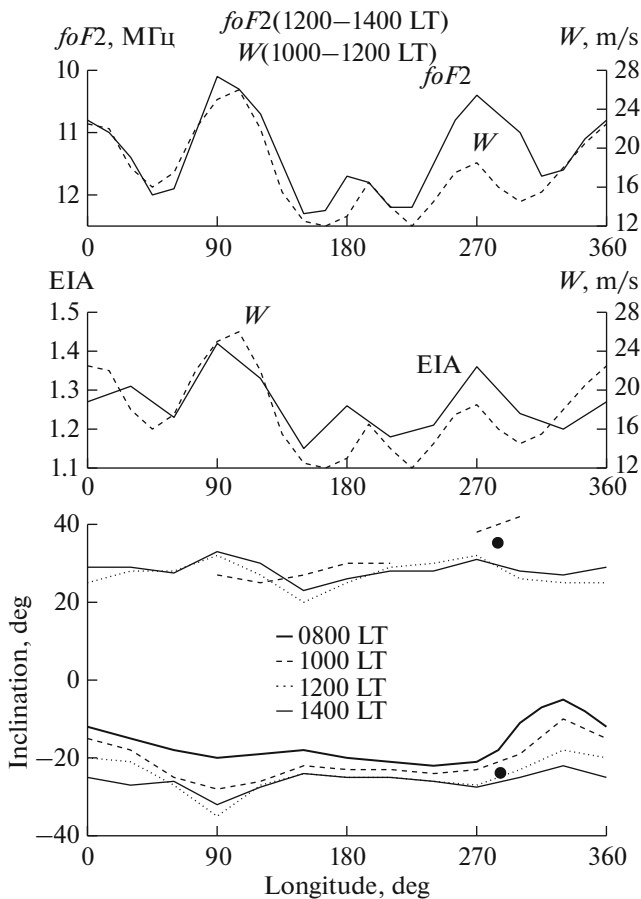
**Fig. 3.** Longitudinal variations of *foF*2 and *W* (top), the EAI and *W* (middle), and crest positions for different local hours (bottom). The circles show the crest positions for the Alouette satellite data at 1400 LT (Sharma and Hewens, 1976).

solstices. For example, according to Alouette-1 data for October 1962−December 1964 at American longitudes of 90°−55° W in the summer months, the northern crest was ~10° DIP farther from the equator than the southern crest (Sharma and Hewens, 1976). For comparison, the difference in crest position in the longitudinal sector of 300° at 1400 LT in Fig. 2 is only 3°−4°. Even smaller differences (2°−3°) were recorded in the study cited above (Zhao et al., 2009). The *foF*2 value in the crests of the equatorial anomaly reaches the maximum values of 14−15 MHz by 1400 LT and remains the same during the daytime.

Only one example of the *foF*2 distribution for 1200 LT was found, which can be directly compared with the distribution for 1200 LT in Fig. 1. It was obtained from COSMIC data for June and refers to the low solar activity of $F_{10.7} = 76.4$ (Zeng et al., 2007). It is all the more interesting that this structural distribution is in good agreement with Fig. 1. This means that its structure at noon is determined by the same factors, despite the large differences in EA behavior at high and low solar activity. Note that the equatorial *foF*2 trough at

1200−1400 LT at all longitudes is strictly at the geomagnetic equator in both cases. Conversely, Liu and Watanabe (2008) obtained the ion-density distribution for 1200 LT in June according to CHAMP satellite data reduced to the height of 400 km. This distribution is much closer to the IK-19 data in geophysical conditions, because it also relates to high solar activity, but it corresponds much worse to the *foF*2 distribution in Fig. 1. Therefore, different data (for different seasons) should be compared in a separated paper.

Consider the longitudinal variations of the daytime EA parameters. Longitudinal *foF*2 variations at the equator were first detected according to the IK-19 data (Karpachev, 1988). Top panel in Fig. 3 shows the *foF*2 variations above the equator averaged for 1200−1400 LT with steps of 30° longitude. It is well known that they are determined by variations in the plasma vertical drift velocity *W* (the dashed curves in Fig. 3). The *W* variations above the equator are given for 1000−1200 LT, i.e., during the period of EA development. (Positive values indicate upward drift). They were obtained from ROCSAT-1 for summer (May−August) quiet conditions in 1999−2004 at high solar activity (Fejer et al., 2008). Figure 3 shows that, indeed, the *foF*2 variations follow the *W* variations, except for the longitudinal sector of 240°−300°, where *foF*2 is much smaller than might be expected. At the same time, the electron density in this longitudinal sector is lower at all latitudes, including the anomaly crests. As a result, the *foF*2 ratio at the crest maxima and above the equator at a longitude of 270° is smaller than at a longitude of 90°, although not by much. Therefore, we can state that the daytime EA intensity (EAI) in the American longitudinal sector is a little less than that in the Asian longitudinal sector. The EA is least developed during the daytime at longitudes of 150°−210°. Once again, let us recall the aforementioned work (Thomas, 1968) in this regard.

It should also be noted that all of the considered parameters show four harmonics in longitude with close maxima and minima. This fact is reflected in the recently intensively researched, wave-4 concept (e.g., Ram et al., 2009). It assumes that the lower atmosphere influences the ionosphere of the *E* region and, consequently, the value of the vertical drift (e.g., Pancheva and Mukhtarov, 2012 and references therein). A continuous curve in the middle of Fig. 3 shows longitudinal variations of the EAI as the ratio of *foF*2 in the crests to *foF*2 in the equatorial trough, i.e., $EAI = foF2_C/foF2_E$. The *foF*2 values in the northern and southern crests of the anomaly were averaged. The EAI variations were also obtained via averaging of the data for 1200−1400 LT. They are similar to the *W* variations and also show 4th harmonic dominance.

The bottom panel of Fig. 3 presents the longitudinal variations of EA crest positions for 0800, 1000, 1200, and 1400 LT. Their dynamics during the period of EA development have already been partially dis-

cussed. First, the winter crest of the anomaly appears. As the EA develops, it moves away from the equator at all longitudes and increases in magnitude. At the same time, the crest position at noon very strongly changes with longitude, from 18° $I$ in the American sector to 32° $I$ in the Asian sector. These changes are associated with the EAI, as noted above. The summer (northern) crest starts to appear only at 1000 LT, and only at noon it is formed at all longitudes. Its position also changes quite strongly with longitude. The dashed line in Fig. 2 at longitudes of 270°−300° in the Northern Hemisphere shows the position of a low-latitude and fairly pronounced $foF2$ maximum. It can be considered an EA crest, which significantly complicates the analysis. Note also that the northern crest at 1000 LT is farther from the equator at longitudes of 150°−180° than at 1200 LT. All of this is due to the complex dynamics of the formation of the northern crest at a background of a low-latitude $foF2$ maximum. Both crests still move a little farther from the equator at 1400 LT, not at all longitudes but on average. The distance between the crests at 1400 LT in terms of magnetic inclination is 65° $I$ in the longitudinal sector of 90°, 58° $I$ at longitude 270°, and only 47° $I$ at longitude 330°. The latter values are inconsistent with the Alouette satellite data for the American sector (55°−90° W), according to which the EA width was 65° $I$ at high solar activity (58° $I$ at low) (Sharma and Hewens, 1976). The circles in Fig. 3 show the positions of both crests from this work for 1400 LT for the summer solstice and low solar activity. The data are in good agreement in the Southern Hemisphere. According to Alouette, the northern crest is exactly in the middle between the "true" EA crest and the low latitude maximum observed at 0800 LT, which is clearly not associated with the EA. This suggests that the crest and low-latitude $foF2$ peak form a common maximum at low activity, even at noon.

## 4. EVENING EA INTENSIFICATION

After the EA development reached its maximum at 1400 LT, it was in a relatively stable condition for several hours. The situation changes rapidly in the evening hours. In the evening, the equatorial ionosphere is subject to competing factors: vertical drift and diffusion, recombination, and neutral wind (Balan and Baily, 1995). Therefore, the EA dynamics at this time are quite complex. Figure 4 shows the $foF2$ distribution at 1600, 1900, 2000, and 2200 LT, and Fig. 5 shows the latitudinal $foF2$ profiles at 1800, 2000, and 2200 LT in the longitudinal sectors 90° and 300°. Both figures clearly show the EA dynamics in the evening hours. The first map describes the situation in the equatorial ionosphere at 1600−1700 LT. It is not much different from the situation at 1400 LT. The EA is still well developed. The electron density at the crest maxima remains high (13−14 MHz). The second map describes the situation at 1800−1900 LT. At this time, the electron density at the low-/midlatitudes decreases by the eve-

ning, with ionospheric illumination decreasing due to recombination. The electron density in the crests decreases and remains almost constant above the equator. Therefore, the rate of EA development slows slightly as compared to the daytime hours. The bottom panel of Fig. 6 shows the longitudinal variations in the crest positions. It can be seen that both crests are as close to the equator as possible at almost all longitudes at 1900 LT. Figure 5 shows the latitudinal $foF2$ profiles at 1800 LT in order to demonstrate the rapidity of the decrease in electron density by 2000 LT. The southern (winter) crest at 2000 LT becomes much larger than the northern crest at a longitude of 90°, and they are the same at a longitude of 300°. This crest behavior in summer conditions was observed from ground-based data already by Thomas (1968). The vertical upward drift velocity at 1800−1900 LT increases, and the drift direction reverses after 2000 LT. Both of these effects strengthen the EA (Balan and Baily, 1995). When the EA strengthens, $foF2$ above the equator decreases, because it is carried by the drift and diffusion to the crest maxima and reaches a minimum by 2200 LT (Fig. 5). The crests move away from the equator (Fig. 6), and their magnitudes are maintained at a high level by this process, which is particularly well seen in the example of the southern crest in the longitudinal sector of 90°. The average $foF2$ values at the crest maxima in the evening do not differ much from the daytime values, but they reach 15−16 MHz on some days.

In the evening, as well as at noon, the entire EA changes structure quite strongly with longitude (Fig. 6). However, the variations are quite different, and not only because there is no four-mode structure in them. The longitudinal $foF2$ variations above the equator and EAI averaged for 1900−2000 LT are presented at the top and in the middle of Fig. 6, respectively. The dashed curve shows changes in plasma vertical drift velocity $W$. They were obtained from the ROCSAT-1 satellite data for summer conditions under high solar activity (Fejer et al., 2008). Numerical values of $W$ were digitized from a color figure (Fig. 4) of this paper for ~1900 LT and may not accurately estimate the drift velocity variations. Nevertheless, it can be seen from Fig. 6 that the EAI variations, as well as during EA formation (Fig. 3), are quite clearly defined by the vertical plasma drift. The delay is 1.0−1.5 h. It is mainly related to the diffusion time (Moffett, 1979). Again, the $foF2$ variations do not follow $W$ variations only in the American longitudinal sector of 270°−330°: the electron density in the $F2$ layer maximum decreases instead of increases in $foF2$ with a decrease in $W$. Once again, it decreases at all latitudes in this longitudinal sector, including the crests of the anomaly (Fig. 5). As a result, the ratio of $foF2$ in the crests and above the equator shows a less developed EA; thus, the correlation of $W$ and EAI is not disturbed in the American sector. The EA develops even more weakly at Asian longitudes. That is, the situation is the opposite of that observed during the daytime (Fig. 3). Next, the EA is
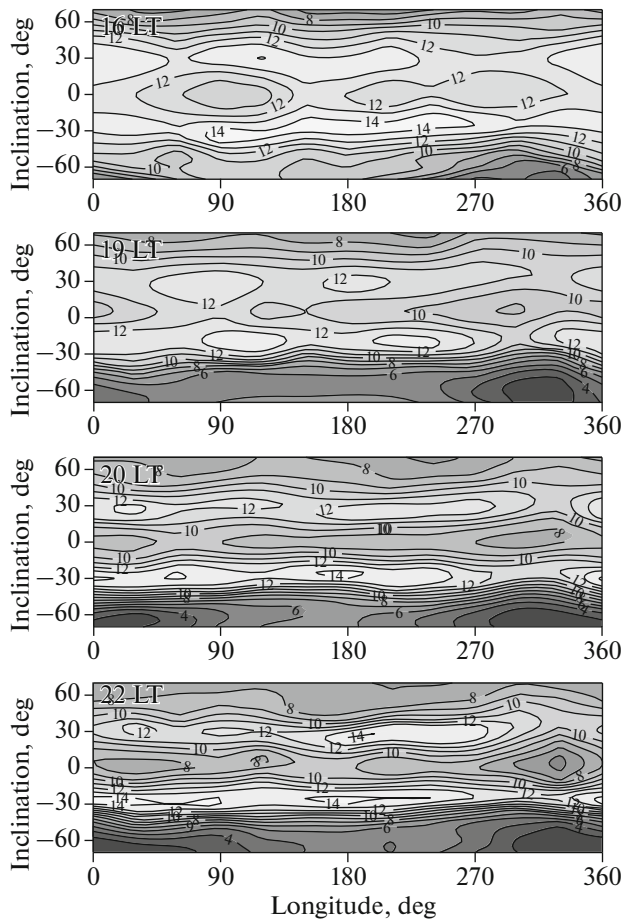
**Fig. 4.** Distribution of *foF*2 at 1600, 1900, 2000, and 2200 LT.

most strongly developed at longitudes 0° and 180°. After 2000 LT the EA becomes slightly stronger yet at all longitudes, although it has almost no effect on the crest position. It should be noted that the closest crests to the equator are at 1900 LT. A strong EA asymmetry in crest magnitude in Asia and in crest position in America (Figs. 5 and 6) is observed at 2000−2200 LT.

Since the vertical drift velocity changes greatly with longitude, not only *foF*2 but also the entire electron density profile will change with longitude. Figure 7 shows the *N*(*h*) profiles for three characteristic longitudinal sectors. In order to avoid day-to-day variations, they were obtained from the averaging of several profiles in the 1900−2000 LT range in the longitudinal sectors of 60°−90°, 180°−210°, and 300°−310°. The profiles were selected for quiet geomagnetic conditions in the latitude range ±5° *I*. Figure 7 shows that the *foF*2 variations are maximal and the *hmF*2 values are minimal at longitudes of 60°−90°. In the longitudinal sector of 180°−210°, *foF*2 is smaller and the *F*2 layer is much higher. As a result, the electron density in the entire topside ionosphere is high. All of this is explained by the well-known effect of vertical plasma drift: the higher the upward drift velocity is, the more

strongly the electron density is carried to higher altitudes. Therefore, it decreases at the *F*2-layer maximum and increases at higher altitudes. The *F*2 layer rises in this case. The vertical drift velocity is as low as at longitudes of 60°−90° in the longitudinal sector of 300°−310°, but there are minimal *foF*2 values at all latitudes. Consequently, they are determined by some other mechanism, most likely by the action of neutral wind and thermosphere composition, i.e., a reduction of $O/N_2$. However, calculations are required to answer this question.

## 5. EA DECAY

Consider the dynamics of the EA during its decay. Figure 8 shows the *foF*2 distributions at 0000, 0200, and 0400 LT, and Fig. 9 presents the latitudinal *foF*2 variations for these local hours in longitudinal sectors 90°, 180°, and 300°. The longitudinal sector 180° is shown, because it becomes specific again during EA decay. It begins to decay after the evening peak in the vertical drift and the associated EA intensification. The decay begins slowly; thus, the anomaly is still quite well developed even at midnight (Figs. 8 and 9). This contrasts sharply with the EA behavior at low activity, when it almost disappears already by 1800−1900 LT. This was clearly shown in (Liu et al., 2007; Ram et al., 2009; Xiong et al., 2013). The EA decay can be clearly seen in Fig. 9 when compared to the reference latitudinal profile at 2200 LT. After 2200 LT, the EA crests move toward the equator and decrease in magnitude, which is especially evident at longitudes of 90° and 300°. In the longitudinal sector of 180°, the crests continue to move toward the equator even after midnight, and only then do they sharply decrease in magnitude. In the longitudinal sector of 90° and 300°, conversely, the crests move away from the equator from midnight to 0200 LT. At American longitudes, this movement continues; thus, the *foF2* maximum is at latitude ~33° *I* at 0400 LT in the Southern Hemisphere and is almost at midlatitudes ~50° *I* in the Northern Hemisphere. This is too far for a normal EA crest created by the fountain effect. Both crests are also farther from the equator at 0400 LT than at 0200 LT in the longitudinal sector of 180°, while they are a slightly closer in the longitudinal sector of 90°. After midnight, the southern crest decays much faster than the northern one, i.e., there is an EA asymmetry inverse to that observed during EA development. At 0400 LT, the southern crest is very small, much smaller than the northern crest (maximum). This is a well-known fact (e.g., Rao and Jogulu, 1979; Zhao et al., 2009). It was also argued that the EA is longer in the American sector (Walker, 1981). However, it is difficult to draw such a conclusion from Figs. 8 and 9, unless, of course, one takes into account the fact that there is no southern crest at 0400 LT in the longitudinal sector 330°. However, this is already at the Atlantic longitudes.
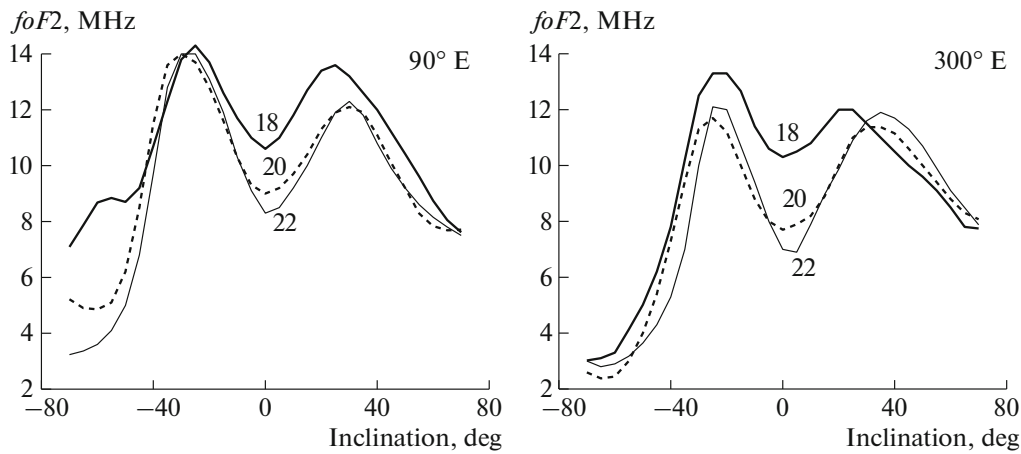
**Fig. 5.** Latitudinal *foF*2 variations at 1800, 2000, and 2200 LT in the longitudinal sectors of 90° and 300°.

Figure 10 shows the variations in EA crest positions during EA decay. By midnight, the crests already shifted slightly toward the equator in comparison with the maximum development at 2000−2200 LT. The position of the southern crest at this time differs from the position at 0200 and 0400 LT by only 2°−3°, which is within the accuracy of its determination. However, the further behavior of the southern crest clearly depends on longitude. In the Eastern Hemisphere, it is farther from the equator at 0200 LT than at 0400 LT, while, conversely, it is closer to the equator in the Western Hemisphere. The crest position depends on the action of neutral wind, which is especially important when the fountain effect is weakened. It can then be assumed that the night wind to the equator was stronger at 0200 LT than at 0400 LT in the Eastern Hemisphere and vice versa in the Western Hemisphere. This is difficult to verify, because the neutral wind model HWM reproduces wind speed in the Southern Hemisphere with large errors (e.g., (Karpachev and Gasilow, 2001).

The northern crest undergoes much stronger variations with longitude. At 0200 LT, the northern crest, like the southern one, is closer to the equator than at midnight only in the longitudinal sector of 180°−270°, i.e., the EA is most underdeveloped under these conditions. At other longitudes, the northern crest moves away from the equator after midnight. At longitudes of 270°−300°, the *foF*2 maximum at 0400 LT is at a latitude of 52° *I*. It is still unknown to what extent this maximum is related to the "normal" EA crest. Therefore, it is formally indicated in Fig. 10 as an EA crest. Note that the longitudinal variations of the crest position in the Northern Hemisphere are similar in shape to longitudinal *foF*2 variations in the nighttime midlatitude ionosphere (e.g., Klimenko et al., 2016). This applies to both crests, which once again indicates a neutral wind rather than an electric field generating the EA.

## 6. DIURNAL EA VARIATIONS

Consider briefly the diurnal variations of EA characteristics, because they have already been analysed in general above. Figure 11a shows the diurnal variations of the EAI. They were obtained via the separate averaging of data for longitudes of 90°−120° and 270°−300°. The ver-
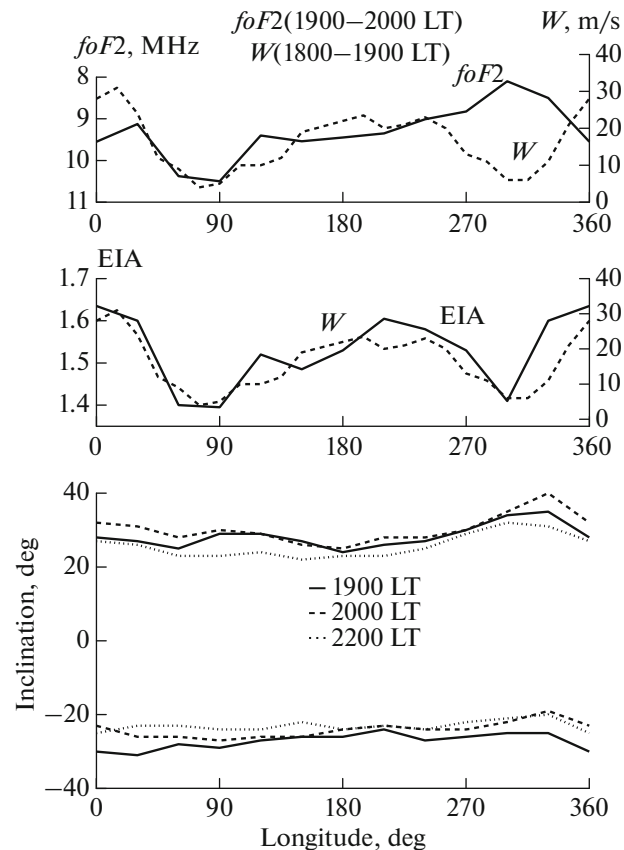


**Fig. 6.** Longitudinal variations of *foF*2 and *W* (top), the EAI and *W* (middle), and crest positions for different local hours (bottom).
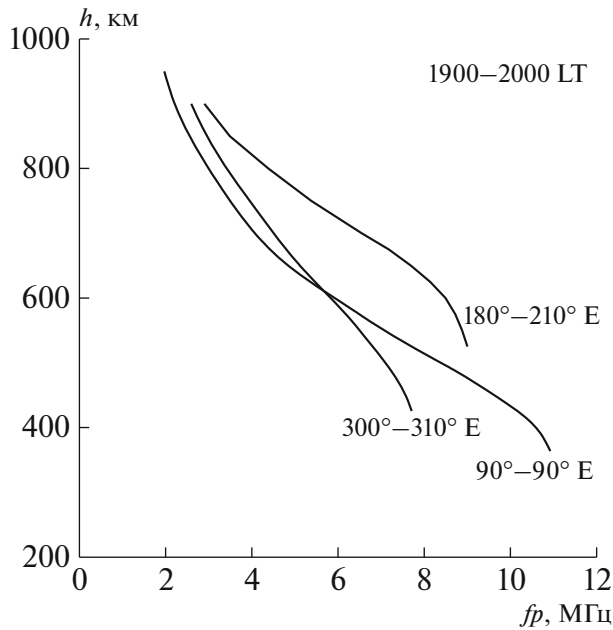
**Fig. 7.** $N(h)$ profiles of the upper ionosphere for 1900–2000 LT in the characteristic longitudinal sectors.
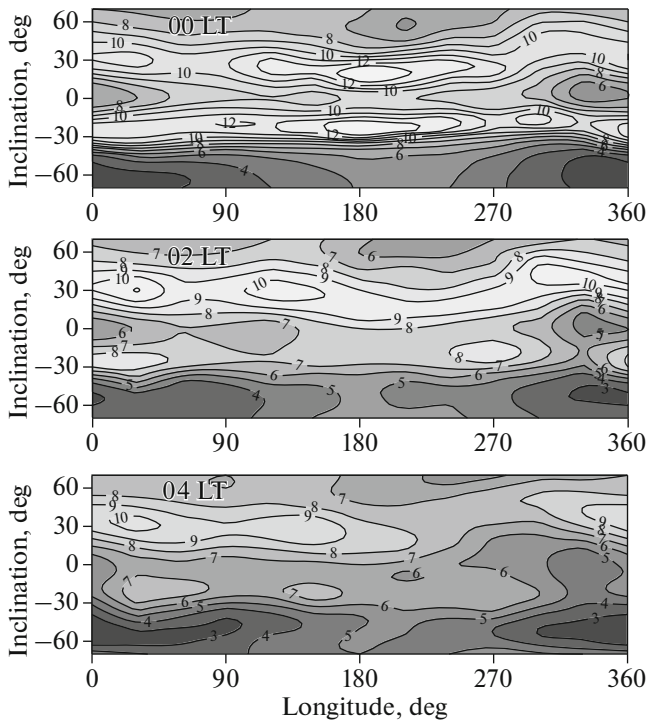


**Fig. 8.** Distribution of $foF2$ at 0000, 0200, and 0400 LT.

tical plasma drift variations obtained for summer conditions based on the ROCSAT-1 data (Fejer et al., 2008) are also presented (Fig. 11b). The EA begins to form at 0800 LT with the emergence of the southern crest (Fig. 11d). It dominates over the northern crest up to 1400 LT. Therefore, the EAI was calculated

during this period as the ratio of $foF2$ in the southern crest maximum to the $foF2$ in the equatorial trough. The EA develops, and both EA crests form at 1000 LT. It is clear that all of this happens after the vertical plasma drift velocity changes to the upward direction. At Western Hemisphere longitudes (dashed curve for $270°–300°$), the EAI increases almost monotonically up to 1700 LT with a small maximum at 1400 LT. This maximum is expressed much more clearly in the longitudes of the Eastern Hemisphere ($90°–120°$). Obviously, it is related (with a quite-understandable delay) to the local maximum plasma drift velocity at 1000–1100 LT. This $foF2$ maximum was recorded earlier from the ISS-b satellite data for August–December 1979 (Matuura, 1981), and it was in the sector of $90°–120°$ that this maximum manifested itself most strongly. The EAI maximum at noon is associated with the noon decrease in $foF2$ (Fig. 11c), which is observed as a so-called bite-out from the longitudes of India (Rao, 1963). In the American longitudinal sector, the next local maximum is observed at 1700 LT. It was initially doubted. Therefore, the data for this sector were carefully double-checked. In addition, it was found that this maximum was also observed from ground data obtained for the $75°$ $W$ meridian in June at high solar activity (Rush et al., 1969). Therefore, it was confirmed, and it is now necessary to find its cause. The variations in EA crest positions in Fig. 11d were obtained via the averaging of data for all longitudes. It can be seen that the southern crest appears at a latitude of $16°$ $I$ and that it moves away from equator to $28.5°$ $I$ by 1400 LT as the EA develops. The northern crest is a few degrees farther from the equator all day. However, it starts at a too high latitude ($30°$ $I$) because, as shown above, it forms at the background of a low-latitude $foF2$ maximum. It can be assumed that $30°$ $I$ is a joint latitude for the peak associated with the neutral wind and for the crest of the anomaly generated by the fountain effect. The northern crest is also as far away from the equator as possible at 1400 LT. Therefore, the northern crest is always farther from the equator, i.e., there is moderate EA asymmetry, which increases from 2000 LT to 0400 LT. Almost the same asymmetry was observed according to the CHAMP satellite for the June solstice at high solar activity (Xiong et al., 2013). The circle in Fig. 11d shows the position of the northern crest obtained via averaging of the TEC data obtained at the Lunping Observatory ($25°$ N, $121°$ E) at high solar activity (Huang and Cheng, 1996). The agreement with the northern crest averaged for all longitudes is good. It is stated that the position of the northern crest in summer does not depend on solar activity. However, it seems that the problem of the dependence of the EA crest position on longitude, season, and solar activity should be considered more deeply.

It can also be seen in Fig. 11c that, as the EA develops, $foF2$ increases in both crests (to ~14 MHz) and decreases above the equator. The reverse process, in
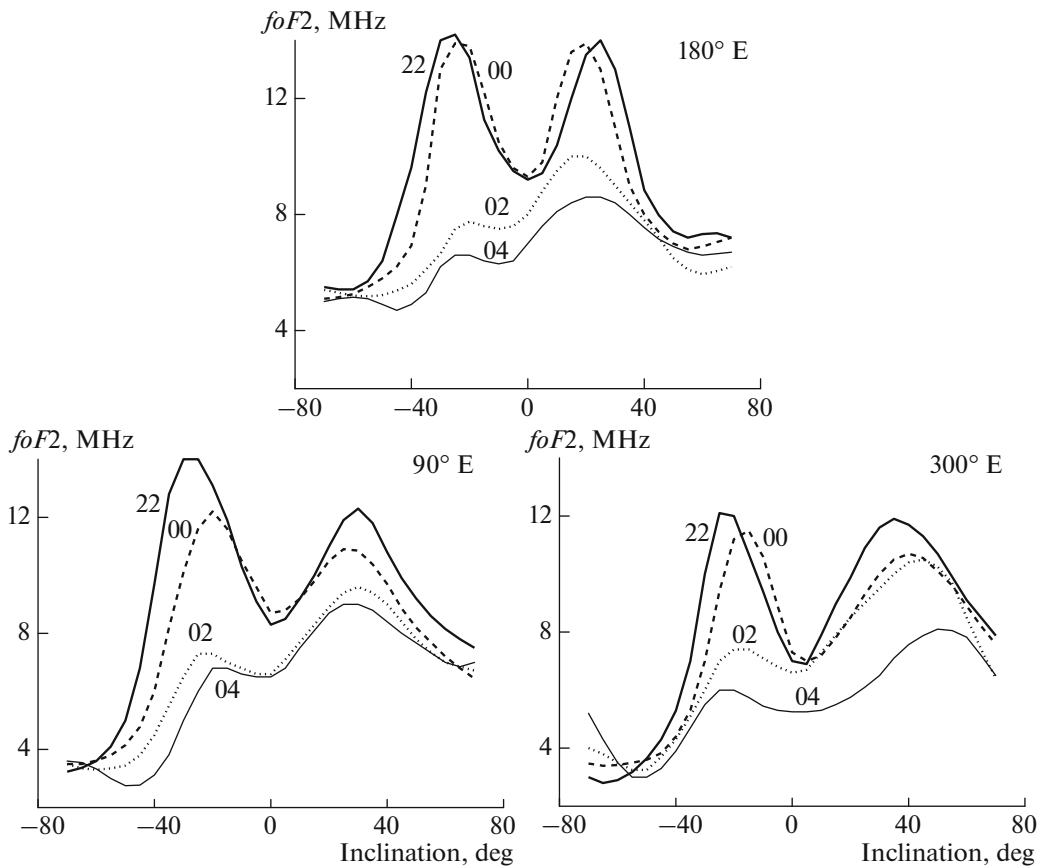
**Fig. 9.** Latitudinal *foF*2 variations at 2200, 0000, 0200, and 0400 LT in the characteristic longitudinal sectors of 90°, 180°, and 300°.

which the EA weakens slightly and by 1900 LT reaches the local minimum, is observed after 1400 LT. It was shown above that the electron density in the crests decreases by 1800−1900 LT and changes little above the equator. Therefore, the EAI decreases in comparison with daytime hours. This is clearly due to the local minimum *W* at 1700 LT. The EAI then quickly reaches a maximum of EAI = 1.58 at 2000 LT at all longitudes, i.e., with a delay of 1.5−2.0 h after an evening peak of the vertical plasma drift velocity. The IK-19 data do not make it possible to determine this delay more accurately. The EAI then drops slightly and then reaches an absolute maximum of 1.65 at 2200 LT. (As shown above, these values are slightly higher at a longitude of 180°). This maximum is associated with a downward drift (Fig. 11b). The downward drift carries plasma along magnetic field lines again at crest latitudes, and the electron density above the equator continues to decrease by morning (Balan and Baily, 1995). The EA crests are the farthest away from the equator at 2000−2200 LT. The total EA width reaches 56° *I*. After 2200 LT, the EA decreases by morning hours with another local maximum at 0200 LT. Note that, since the northern crest of the anomaly is the largest in the EA decay phase, the EAI was calculated based on its value at that time. The average position of the south-

ern crest after midnight is almost unchanged, and the northern crest moves away from the equator. However, as was shown above, the crest behavior is very much dependent on longitude. In the Asian sector, the northern crest after midnight and the southern crest at 0200 LT are always farther away from the equator than at midnight. The crest motion from the equator is con-
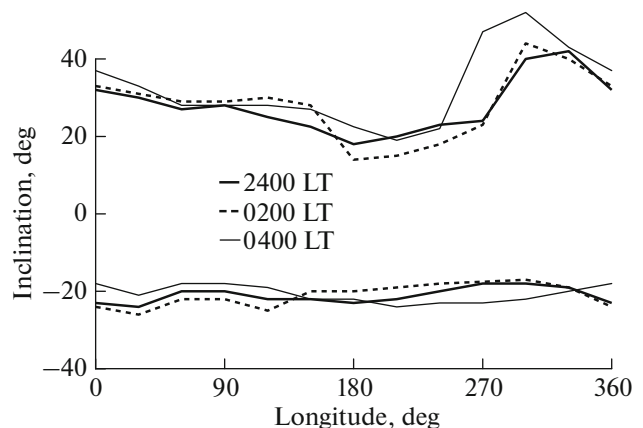


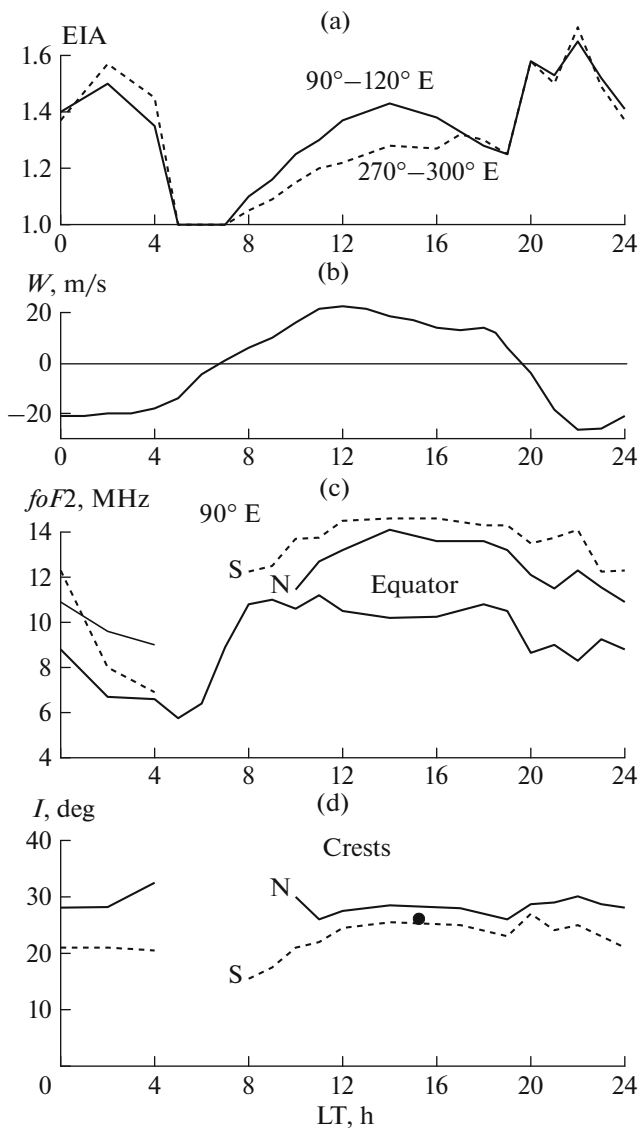**Fig. 10.** EA crest position variations at 0000, 0200, and 0400 LT.

**Fig. 11.** Top down: diurnal EAI variations in longitudinal sectors of 90°−120° and 270°−300°, vertical drift velocity $W$ (Fejer et al., 2008), $foF2$ values in crests and above the equator, and crest positions. The circle indicates the northern crest position at longitude 121° (Huang and Cheng, 1996).

sistent with ground-based observations made in the Asian sector by Walker et al. (1994). The authors argued that there is a resurgence of EA crests around 0300 LT at high solar activity in any season. According to the authors, this is associated with the known, post-midnight increase in electron density at the midlatitudes, which is then transferred to the equator by the neutral wind (e.g., Farelo et al., 2002). In the American longitudinal sector, both crests are farther away from the equator at 0400 LT than at midnight, i.e., an EA increase is also observed. This is consistent with the conclusions made by Yizengaw et al. (2009), in which an EA maximum was first observed on April 27, 2003, at 2000 LT, followed by a minimum at 2330 LT,

and then again by a well-developed EA up to 0400 LT according to the TEC TOPEX data at longitude 80° *W*. An EA increase at 0200−0300 LT was also found as a result of the statistical analysis of the EA based on COSMIC data under low solar activity (Yue et al., 2015). Therefore, this is a rather clearly defined feature of EA dynamics. However, as shown above, the electron density peaks at crest latitudes at 0200−0400 LT, at least at American longitudes, are related to the action of the neutral wind rather than the electric field generating the EA. Therefore, this should be taken into account when a conclusion is drawn about EA resurgence.

## 7. DISCUSSION AND CONCLUSIONS

A detailed pattern of $foF2$ variations in the EA region for the summer solstice at high solar activity was constructed for the first time. This was only possible due to the unique data from the Interkosmos-19 satellite, which provided a global array of data on the electron density in the topside ionosphere, including the $foF2$ and $hmF2$ values. The obtained pattern is the most complete, since it describes almost all EA manifestations under summer conditions, including the diurnal and longitude variations in the EAI and its crest positions. The constructed pattern is quite consistent with the individual results obtained earlier. In particular, it has long been established that the EA begins to form by 0800−0900 LT and is quite well developed at midnight with high solar activity, in contrast to low solar-activity conditions, when it decays by 1900−2000 LT. First, the winter (southern) crest of the EA forms. The EA development is clearly associated with the change of direction of the electric field to the east, after which the vertical plasma drift $W$ is directed upward and the fountain effect is activated. The northern summer crest appears only by ~1000 LT and lags behind for a long time; thus, it is a little smaller than the winter crest even at 1400 LT. During the decay period, conversely, the northern crest exists for longer than the southern crest, up to 0400 LT. This behavior is also well known and is inherent with both high and low solar activity. This is most clearly demonstrated by the COSMIC data under low and medium activity (Luan et al., 2015) and by the TEC data at high solar activity (Zhao et al., 2009). The IK-19 data show that the more complex dynamics of the northern crest is associated with the fact that it forms at a low-latitude $foF2$ maximum. This maximum is easy to confuse with the crest, which is probably explained by differences in position of the northern crest according to different data. The IK-19 data confirm that there is a more pronounced local EAI maximum at 1400 LT in the Eastern Hemisphere than in the Western Hemisphere. Conversely, the weak local EAI maximum detected at 1700 LT was identified in the Western Hemisphere but was not observed in the Eastern Hemisphere. The EA is most weakly expressed at

1900 LT due to the local minimum in *W*. The intensity then increases rapidly. It is usually considered that the EAI reaches its maximum at 2000 LT. This is much later than with low solar activity (at 1600−1700 LT), which was clearly shown by Ram et al. (2009). However, the IK-19 data show a double maximum at 2000 and 2200 LT. The former is definitely due to an evening peak in the vertical plasma drift velocity, while the latter is obviously associated with a downward reversal of drift velocity, after which the EA increases. The average EA width at 2000−2200 LT reaches a maximum of 56° *I*. In the literature, there has been a long discussion about whether the EA is more developed in the Asian or American longitudinal sector. The IK-19 data make it possible to answer this question: during the period of EA development, it is the most strongly developed in the Asian sector, a little bit less in the American sector, and the weakest at longitudes 180°−210°. At this time, a strong fourth harmonic is observed in longitude variations of EA parameters. In the evening, conversely, the EA is most strongly developed at longitudes 180°−210° and least developed in the Asian and American sectors. During the EA decay, the dependence on longitude was not clearly manifested at 0200−0400 LT, i.e., it cannot be said, as is often done, that the EA exists longer in the American sector. The EAI varies according to the usual scheme, i.e., as the anomaly increases, the electron density decreases above the equator and increases in the crest maxima, and they move away from the equator. The crest positions, especially in winter, strongly depend on longitude, up to 15° *I*. This also implies a strong EA asymmetry. However, on average, the northern crest during the daytime is only 3°−4° *I* farther from the equator than the southern one. This distance increases significantly after midnight, but the neutral wind effect apparently is dominant over the fountain effect at this time.

The EA characteristics are very different at low and high solar activities. In recent years, a huge amount of data on TEC and radio occultation has been obtained at low solar activity, which obviously can also provide a complete pattern of variations of EA characteristics. Comparison of the EA pattern at high and low solar activities will, in turn, allow a much deeper understanding of the mechanism of EA formation. Since there is no such possibility, a comparison can be made on separate aspects of this pattern. This was partially done in this article.

The construction of a complete and detailed pattern of the EA dynamics does not mean that there are no problems remaining. We note the most obvious ones. For example, it is assumed that there is no EA in the period 0500−0700 LT. However, the IK-19 data sometimes show small crests even at 0600 LT. The northern crest forms at the background of a low-latitude maximum of electron density. Therefore, we are likely to observe their joint dynamics, which is especially true for the period of the EA decay, when the *foF*2 maximum in the Northern Hemisphere is at too high of a latitude (52° *I*). The geomagnetic equator is far to the south of the geographical one in the American longitudinal sector. This is probably why the EA behavior here is very complex, as shown above. All of these problems require further research.

## REFERENCES

Appleton, E.V., Two anomalies in the ionosphere, *Nature*, 1946, vol. 157, p. 691.

Balan, N. and Bailey, G.J., Equatorial plasma fountain and its effects: Possibility of an additional layer, *J. Geophys. Res.*, 1995, vol. 100, no. 11, pp. 21421−21432.
https://doi.org/10.1029/95JA01555

Chen, Y., Liu, L., Le, H., Wan, W., and Zhang, H., Equatorial ionization anomaly in the low-latitude topside ionosphere: Local time evolution and longitudinal difference, *J. Geophys. Res.*, 2016, vol. 121, pp. 7166−7182.
https://doi.org/10.1002/2016JA022394

Eccles, D. and King, J.W., A review of topside sounder studies of the equatorial ionosphere, *Proc. IEEE*, 1969, vol. 57, no. 6, pp. 1012−1018.

Farelo, A.F., Herraiz, M., and Mikhailov, A., Global morphology of night-time NmF2 enhancements, *Ann. Geophys.*, 2002, vol. 20, no. 11, pp. 1795−1806.

Fejer, B.G., Jensen, J.W., and Su, S.-Y., Quiet time equatorial F region vertical plasma drift model derived from ROCSAT-1 observations, *J. Geophys. Res.*, 2008, vol. 113, A05304.
https://doi.org/10.1029/2007JA012801

Hopkins, H.D., Longitudinal variation of the equatorial anomaly, *Planet. Space Sci.*, 1972, vol. 20, no. 12, pp. 2093−2098.

Huang, Y.-N. and Cheng, K., Solar cycle variations of the equatorial ionospheric anomaly in total electron content in the Asian region, *J. Geophys. Res.*, 1996, vol. 101, no. 11, pp. 24513−24520.

Karpachev, A.T., Characteristics of the global longitudinal effect in a nighttime equatorial anomaly, *Geomagn. Aeron.*, 1988, vol. 28, no. 1, pp. 46−49.

Karpachev, A.T., Diurnal and longitudinal variations of the structure of an equatorial anomaly during equinoxes according to Intercosmos-19 satellite data, *Geomagn. Aeron. (Engl. Transl)*, 2018, vol. 58, no. 3, pp. 407−419.

Karpachev, A.T. and Gasilov, N.A., Zonal and meridional wind components derived from Intercosmos-19 hmF2 measurements, *Adv. Space Res.*, 2001, vol. 27, nos. 6−7, pp. 1245−1252.

King, J.W., Olatunji, E.O., Eccles, D., and Newman, W.S., The integrated electron content in the equatorial ionosphere, *J. Atmos. Terr. Phys.*, 1967, vol. 29, no. 11, pp. 1391−1396.

Klimenko, V.V., Karpachev, A.T., Klimenko, M.V., Ratovskii, K.G., and Korenkova, N.A., Latitudinal structure of the longitudinal effect in the nighttime iono-

sphere during the summer and winter solstice, *Russ. J. Phys. Chem. B.*, 2016, vol. 10, no. 1, pp. 91−99.

Lei, J., Thayer, J.P., and Forbes, J.M., Longitudinal and geomagnetic activity modulation of the equatorial thermosphere anomaly, *J. Geophys. Res.*, 2010, vol. 115, A08311. https://doi.org/10.1029/2009JA015177

Liu, H., Stolle, C., Forster, M., and Watanabe, S., Solar activity dependence of the electron density at 400 km at equatorial and low latitudes observed by CHAMP, *J. Geophys. Res.*, 2007, vol. 112, A11311. https://doi.org/10.1029/2007JA012616

Liu, H. and Watanabe, S., Seasonal variation of the longitudinal structure of the equatorial ionosphere: Does it reflect tidal influences from below?, *J. Geophys. Res.*, 2008, vol. 113, A08315. https://doi.org/10.1029/2008JA013027

Lockwood, G.E.K. and Nelms, G.L., Topside sounder observations of the equatorial anomaly in the 75° W longitude zone, *J. Atmos. Terr. Phys.*, 1964, vol. 26, no. 5, pp. 569−580.

Luan, X., Wang, P., Dou, X., and Liu, Y.C.-M., Interhemispheric asymmetry of the equatorial ionization anomaly in solstices observed by cosmic during 2007−2012, *J. Geophys. Res.*, 2015, vol. 120, pp. 3059−3073. https://doi.org/10.1002/2014JA020820

Lyon, A.J. and Thomas, L., The *F*2-region equatorial anomaly in the African, American and East Asian sectors during sunspot minimum, *J. Atmos. Terr. Phys.*, 1963, vol. 25, no. 7, pp. 373−386.

Matuura, N., Characteristics of global distribution of *foF*2, *Sol. Terr. Environ. Res. Jpn.*, 1981, vol. 5, pp. 35−38.

Moffet, R., The equatorial anomaly in the electron distribution of the terrestrial F-region, *Fundam. Cosmic Phys.*, 1979, vol. 4, pp. 313−391.

Pancheva, D. and Mukhtarov, P., Global response of the ionosphere to atmospheric tides forced from below: Recent progress based on satellite measurements global tidal response of the ionosphere, *Space Sci. Rev.*, 2012, vol. 168, nos. 1−4, pp. 175−209.

Rajaram, G., Structure of the equatorial F-region, topside and bottomside—a review, *J. Atmos. Terr. Phys.*, 1977, vol. 39, no. 9, pp. 1125−1144.

Ram, S.T., Su, S.-Y., and Liu, C.H., FORMOSAT-3/ COSMIC observations of seasonal and longitudinal variations of equatorial ionization anomaly and its interhemispheric asymmetry during the solar minimum period, *J. Geophys. Res.*, 2009, vol. 114, A06311. https://doi.org/10.1029/2008JA013880

Rao, B.C.N., Some characteristic features of the equatorial ionosphere and the location of the F-region equator, *J. Geophys. Res.*, 1963, vol. 68, no. 9, pp. 2541−2549.

Rao, C.S.R. and Malthotra, P.L., A study of geomagnetic anomaly during I.G.Y, *J. Atmos. Terr. Phys.*, 1964, vol. 26, no. 11, pp. 1075−1085.

Rao, M.P. and Jogulu, C., Diurnal development of the equatorial anomaly in the topside ionosphere, *Indian J. Radio Space Phys.*, 1979, vol. 8, pp. 310−317.

Rishbeth, H., The equatorial F-layer: Progress and puzzles, *Ann. Geophys.*, 2000, vol. 18, no. 7, pp. 730−739.

Rush, C.M., Rush, S.V., Lyons, L.R., and Venkateswaran, S.V., Equatorial anomaly during a period of declining solar activity, *Radio Sci.*, 1969, vol. 4, no. 9, pp. 829−841.

Sastri, J.H., Equatorial anomaly in F-region—a review, *Indian J. Radio Space Phys.*, 1990, vol. 19, no. 4, pp. 225−240.

Sharma, R.P. and Hewens, E.J., A study of the equatorial anomaly at American longitudes during sunspot minimum, *J. Atmos. Terr. Phys.*, 1976, vol. 38, no. 5, pp. 475−484.

Thomas, L., The F2-region equatorial anomaly during solstice periods at sunspot maximum, *J. Atmos. Terr. Phys.*, 1968, vol. 30, pp. 1631−1640.

Walker, G.O., Longitudinal structure of the F-region equatorial anomaly—a review, *J. Atmos. Terr. Phys.*, 1981, vol. 43, no. 8, pp. 763−774.

Walker, G.O. and Chan, C.S., The diurnal variation of the equatorial anomaly in the topside ionosphere at sunspot maximum, *J. Atmos. Terr. Phys.*, 1976, vol. 38, no. 7, pp. 699−706.

Walker, G.O., Ma, J.H.K., and Golton, E., The equatorial ionospheric anomaly in electron content from solar minimum to solar maximum For South East Asia, *Ann. Geophys.*, 1994, vol. 12, nos. 2−3, pp. 195−209.

Xiong, C., Lühr, H., and Ma, S.Y., The magnitude and inter-hemispheric asymmetry of equatorial ionization anomaly-based on CHAMP and GRACE observations, *J. Atmos. Sol.-Terr. Phys.*, 2013, vol. 105, pp. 160−169. https://doi.org/10.1016/j.jastp.2013.09.010

Yizengaw, E., Moldwin, M.B., Sahai, Y., and Rodolfo, J., Strong postmidnight equatorial ionospheric anomaly observations during magnetically quiet periods, *J. Geophys. Res.*, 2009, vol. 114, A12308. https://doi.org/10.1029/2009JA014603

Yue, X., Schreiner, W.S., Kuo, Y.-H., and Lei, J., Ionosphere equatorial ionization anomaly observed by GPS radio occultations during 2006−2014, *J. Atmos. Terr. Phys.*, 2015, vol. 129, no. 7, pp. 30−40.

Zeng, Z., Burns, A., Wang, W., Lei, J., Solomon, S., Syndergaard, S., Qian, L., and Kuo, Y.-H., Ionospheric annual asymmetry observed by the cosmic radio occultation measurements and simulated by the TIEGCM, *J. Geophys. Res.*, 2007, vol. 113, A07305. https://doi.org/10.1029/2007JA012897

Zhao, B., Wan, W., Liu, L., and Ren, Z., Characteristics of the ionospheric total electron content of the equatorial ionization anomaly in the Asian−Australian region during 1996−2004, *Ann. Geophys.*, 2009, vol. 27, no. 10, pp. 3861−3873.

*Translated by O. Pismenov*